Magnetic/flow controlled continuous size fractionation of magnetic nanoparticles using simulated moving bed chromatography

Laura Kuger [1], Carsten-René Arlt [1], Matthias Franzreb [*]

Institute of Functional Interfaces, Karlsruhe Institute of Technology, Hermann-von-Helmholtz-Platz 1, 76344, Eggenstein-Leopoldshafen, Germany

ARTICLE INFO

Keywords:
Magnetic chromatography
Magnetic nanoparticles
Simulated moving bed chromatography
Size fractionation

ABSTRACT

The use of magnetic nanoparticles shows a steadily increasing technical importance. Particularly in medical technology disciplines such as cancer treatment, the potential of these special particles is increasing rapidly. Magnetic nanoparticles are particles with a submicron size, and consist mostly of magnetite-containing composites. An important quality parameter of such particles is a particle size distribution as narrow as possible, which can only be obtained to a certain degree by synthesis. Apart from ultracentrifugation, there are so far only methods on an analytical scale to narrow the size distribution as a post-processing step. We present a method based on magnetic chromatography, by which high separation efficiencies at yields of up to 99.9% are achieved. The novel technique is based on a competition between the magnetic interaction of the nanoparticles and the separation matrix, as well as the hydrodynamic forces. Furthermore, the method is extended using a continuous mode, namely simulated moving bed chromatography, to obtain potent space-time yields of up to 2.94 g/(L*h). For those reasons, this novel continuous magnetic chromatography method offers high potential for large-scale refinement of magnetic nanoparticles while fulfilling sophisticated quality criteria for high-technology applications.

1. Introduction

Nanotechnology is a rapidly growing branch in science, which shows great progress in various research areas. A special discipline is the use of so-called magnetic nanoparticles (MNPs), with a rapidly increasing number of applications shown in multiple scientific topics. On a technical level, MNPs are progressingly used for sensor technology [1], separation and extraction techniques [2,3], magnetic bearings [4], catalysis [5,6] and wastewater treatment [7,8]. Especially in medicine, the use of MNPs for cancer therapy shows very promising application areas. These include, for example, magnetic hyperthermia, a therapy method using spatially focused magnetic fields in combination with defined MNPs to offer a very high and unique specificity for tumor treatment [9–11]. Another interesting application is the so-called targeted drug therapy, in which a particularly high specificity for a local application of active substances in a body can be achieved by a suitable functionalization, for example with monoclonal antibodies or other medical agents [11–13]. Further medical applications would be gene therapy with DNA- or RNA-loaded MNPs [14] or in radiological diagnostics [15]. The synthesis of such MNPs is often carried out via precipitation reactions [16], thermal decomposition [17], hydrolysis [18] or microemulsions [19]. In the aforementioned processes, however, it is only possible to obtain a more or less sharp particle size distribution (PSD). However, uniformity is an important quality parameter for MNPs in many applications [17,20–22]. Magnetite and maghemite in particular are processed as ferromagnetic components in MNPs [23]. In order to achieve a narrowing of the PSD, it is possible to perform a size fractionation after the respective synthesis process. In the particle size range on nanometric scale, however, fractionation processes encounter technical difficulties which have so far only been solved for specific cases. There exist batch-wise methods like ultracentrifugation [24–27], but no continuous processes on an industrial scale for fractionation of particles around 100–700 nm in size are known. On a molecular scale, size exclusion can be very effective for fractionation of protein aggregates or particles of a few nanometers in size. Here, the mass transport between the liquid bulk phase and the inner surface of the stationary phase is dominated by convection and diffusion, with convection having a significant effect only in the bulk. In the case of nanoparticles larger than 50 nm, however, mass transport by diffusion becomes increasingly ineffective. This circumstance results in a separation gap, which shows that an efficient and scalable size separation of particles of 100–700 nm

* Corresponding author.
E-mail address: matthias.franzreb@kit.edu (M. Franzreb).
[1] Authors contributed equally.

Nomenclature

CV	Column volume
DLS	Dynamic light scattering
DNA	Deoxyribonucleic acid
ESEM	Environmental scanning electron microscope
FPLC	Fast protein liquid chromatography
HGMS	High gradient magnetic separation
mFFF	Magnetic field flow fractionation
MNP	Magnetic nanoparticle
RNA	Ribonucleic acid
PEEK	Polyetheretherketone
PSD	Particle size distribution
PTFE	Polytetrafluoroethylene
SE	Secondary electrons
SLM	Selective laser melting
SMB	Simulated moving bed
Tris	Tris(hydroxymethyl)aminomethane
UV-VIS	Ultraviolet–visible

is still a major challenge, because a complex superposition of forces occurs in this size range. For these reasons, high-resolution size fractionation of MNPs remains an intensively studied scientific field. Size fractionation in this context refers to selective fractionation of particles with a wide size distribution into two or more fractions that differ among each other in their median particle diameter. On an analytical scale, other innovative methods have already been investigated for this purpose, including microfiltration and ultrafiltration [28,29], acoustic fractionation [30,31] or gel electrophoresis [32]. Furthermore, due to their magnetic addressability, processing of MNPs is widely carried out using so-called high gradient magnetic separation (HGMS) [33,34]. In order to improve fractionation efficiencies in the nanometric size range, additional forces can be superimposed to diffusive, gravitational, hydrodynamic and inertia forces which are always present in liquid particle suspensions. By using a superimposed magnetic field on a field flow separation (mFFF), an analytical size fractionation can be performed [35,36]. This field-flow separation was extended in 1996 by Ohara et al. by using a combination of thin channels and ferromagnetic wires. Ohara et al. were also the first group introducing the term magnetic chromatography for particle retention in such a setup [37,38], demonstrating the huge potential of this technology [39]. Already in the same year, Nomizu et al. [40] adopted this term, but in contrast to Ohara et al. they filled a small column with magnetizable stainless steel beads as a fractionation matrix for the processing of MNPs. In this work, however, the process was not studied for its effectiveness as a size fractionation method. Contrarily, in a previous work of ours, the use of such a magnetized single column for batchwise fractionation of MNPs was extensively investigated. It was found that with the aid of this novel type of chromatography, high fractionation efficiencies for MNPs in the range of 50–400 nm could be achieved [40]. However, the low throughputs of the system, which operated with a low volumetric flow and consisted of a discontinuous mode of operation, continued to be problematic. These challenges were addressed by converting the system from a batch mode to a continuous process by applying the principle of Simulated Moving Bed Chromatography (SMB). Jungbauer et al. were successful in using classical size exclusion SMB for the separation of protein loaded silica nanoparticles with a size of about 70 nm from unbound protein [41] In another approach, a SMB method for nanoparticle separation could be demonstrated in one of our works by separating two nanoparticle types with different susceptibilities from each other [42]. In a recent work, we were able to use such a SMB process for size fractionation of MNPs for the first time [43]. Fractionation was obtained based on the spontaneous magnetization of single domain MNPs without the application of external magnetic fields. Also, in the case of spontaneous magnetization, the intensity of the magnetic interaction with a magnetizable matrix grows with increasing particle size, since larger volume forces will be generated. Therefore, even without an external magnetic field, this effect resulted in a size-dependent retardation of the MNPs in a magnetic chromatography column. However, the process showed limitations when using nanoparticle sizes above 100 nm, which – in case of the low flow velocities required – often resulted in unwanted permanent particle separation within the column. Furthermore, in this process setup only space-time yields of 0.3 g/(L*h) with separation efficiencies of 0.45 could be achieved. This calls for optimization, since alternative methods, such as ultracentrifugation, allow potentially larger quantity flows. In this paper, we aim to address these limitations by introducing a new processing method including the variation of the hydrodynamic force to act as a counterpart to the magnetic force. Furthermore, the throughput of the process as well as its quality and controllability should be increased by the application of an external magnetic field.

2. Separation mechanism

In this work, the separation mechanism for MNPs is based on the competition between magnetic and hydrodynamic forces. Thereby, the spontaneous magnetization of the magnetic cores of the nanoparticles results in a weak attraction towards the column matrix, even without the superposition of an external magnetic field [44,45]. However, the investigated particles consist of a compound including a larger number of magnetic cores with arbitrary spontaneous magnetization. Concludingly, without an external magnetic field, the resulting attractive force is small and difficult to predict with increasing particle diameter. Therefore, in contrast to the work reported in Ref. [43], here an external magnetic field is applied in order to enhance and align the magnetization of the MNPs. In this case, the magnetic force acting onto the MNPs is a volume force, increasing with the cubic of the MNP diameter assuming an ideal spherical shape:

$$F_{mag} \quad \mu_0 V_P \boldsymbol{M} \nabla \boldsymbol{H} \tag{1}$$

$$F_{mag} \sim d_P^3 \tag{2}$$

μ_0 is the magnetic field constant, V_P is the particle volume, d_P is the particle diameter, M is the particle magnetization and H is the magnetic field strength. Meanwhile, under Stokes conditions, the hydrodynamic drag force grows only linearly with MNP diameter, resulting in the force competition shown in Fig. 1.

$$F_{drag} \quad 3\pi\eta_F v d_P \tag{3}$$

$$F_{drag} \sim d_P^1 \tag{4}$$

η_F is the dynamic viscosity of the fluid and v is the relative velocity between the MNP and the fluid. In regards to the chromatography system this superposition implies that the trajectory of a larger MNP which is mainly dominated by the attractive magnetic force is likely to be retarded or even retained within the chromatography matrix. Meanwhile, the trajectory of a small MNP is dominated by the hydrodynamic drag force and the particle exhibits a higher probability to be discharged within the column effluent.

3. Material and methods

3.1. Chemicals and reagents

In this work, a commercially sourced MNP type (nanomag-D 250 nm, micromod Partikeltechnologie GmbH, Rostock, Germany) consisting of magnetite cores enclosed by a dextran (40 kDa) matrix is used. The particles were provided by the manufacturer as a suspension with highly purified water as a continuous phase. The magnetite constitutes a mass

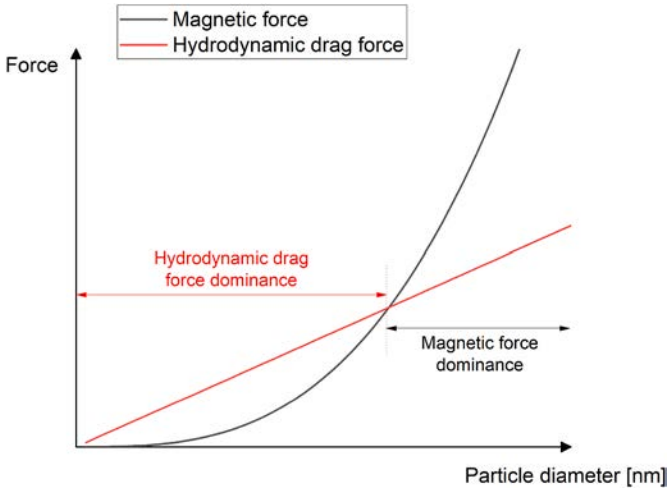

Fig. 1. Qualitative dependencies of the hydrodynamic drag force (red curve) and the magnetic force (black curve) on MNP diameter. The derived theoretical hydrodynamic drag force dominance range is indicated in red and the magnetic force dominance range is shown in black. (For interpretation of the references to colour in this figure legend, the reader is referred to the Web version of this article.)

fraction of about 75–80% and the particles have a total density of 2.5 g/cm^3. The PSD of the MNPs was determined using dynamic light scattering (DLS) technique with a Zetasizer (Zetasizer Nano ZSP, Malvern Instruments, Malvern, England). To describe the PSD, a volumetric density distribution (q_3) was chosen, and a median diameter (D_{50}) of 274 nm was found. The volumetric PSD shows a minimum particle size of 79 nm and a maximum particle size of 955 nm and can be found in Fig. S1 in the SI. The particles were further characterized regarding their magnetic properties using an alternating gradient magnetometer (PMC MicroMag 2900, Princeton Measurement Cooperation, Princeton, USA), the resulting hysteresis curve is depicted in Fig. S2. The particle's specific saturation magnetization of 43 Am^2/kg is in good agreement with the manufacturer's specification. With a specific remanence of 1.57 Am^2/kg, a M_r/M_s ratio of 0.036 results. This ratio is much smaller than that of bulk magnetite, indicating that the magnetite cores, which are randomly embedded in dextran, must be smaller than approximately 20 nm [46]. Also, this finding matches with data from literature, delivering similar remanence and M_r/M_s ratio values for magnetite particles in this size range [47]. The hypothesis of such small particles is confirmed by electron microscopic images (XL30 ESEM-FEG, Philips, Amsterdam, Netherlands) of the particle's magnetite cores, which are shown in Fig. S3. Image analysis reveals a primary particle size of 10–20 nm, with particle diameters not varying substantially. Magnetite particles of such small sizes constitute magnetic single domains [48], which means that they do not form intraparticular domain walls. Each particle instead forms its own domain, with magnetization oriented in uniform directions which results in distinctive material characteristics.

A stainless-steel powder (TruForm 174–2, Praxair Surface Technologies, Ratingen, Germany), fabricated for 3D selective laser melting (SLM), was used as a stationary phase within the magnetic chromatography columns. These particles consist of a chromium-rich (15.7% (w/w)) alloy with 76.0% (w/w) iron content and small amounts of cobalt (3.2% (w/w)), nickel (4.1% (w/w)) and manganese (0.02% (w/w)). Their PSD ranges from 5 to 50 µm with a median diameter (D_{50}) of 31 µm. They show a high saturation magnetization of 135.7 Am^2/kg, a low remanence of 0.36 Am^2/kg, and a coercivity of 698 A/m, indicating good properties for utilization as a matrix material for magnetic fractionation. The corresponding hysteresis curve of the matrix material can be found in Fig. S4.

3.2. Experimental setup

For all experiments, borosilicate glass chromatography columns (Diba Industries Inc, Danbury, USA) with an inner diameter of 6.6 mm and a chromatography bed length of 120 mm (V_{col} 4.105 *mL*) were used. PTFE frits (10 µm in pore size) each at the top and the bottom of the glass column served as filters to prevent the matrix material from being flushed out and to exclude larger impurities. For column packing, the matrix material was wetted with 20% (v/v) ethanol and the excess was removed to eliminate impurities and narrow the size distribution. The slurry was replenished and the procedure was repeated three times. The steel particle suspension was then transferred into the column while ensuring a homogenous and fast flow to avoid the formation of dead volumes and axial size fractionation effects. Afterwards, the chromatography bed was compressed by connecting the column to a pumping system and increasing the flow step by step with 20% (v/v) ethanol as eluent before equilibrating the column with degassed 1 mM TRIS buffer (pH 9.5). Column porosity and peak asymmetry were determined by injecting 100 µL of 1% (v/v) aqueous acetone solution and analyzing the resulting retention time and peak width. A peak asymmetry in the range of 1.0–1.5 was considered acceptable.

A Helmholtz coil arrangement including four copper coils with an average diameter of 75.8 mm was used for the generation of the magnetic fields. By adjustment of the number of windings, a nearly homogeneous field on the chromatography column's central axis was achieved. The magnetic field was controlled at will by applying electrical current using conventional laboratory power supply units (RNDLab, Distrelec Deutschland GmbH, Bremen, Germany). As expected, the induced magnetic flux density showed a linear dependence on the current applied. For instance, an electrical current of 1 A resulted in a magnetic flux density of 6.8 mT on the central axis of the Helmholtz coil arrangement, and thus a magnetization of the steel particles in the column. This again led to the generation of strong field gradients around the steel particles, which act on nanoparticles flowing past.

3.2.1. Single column studies

Preliminary, single column studies were executed using a fast protein liquid chromatography (FPLC) system (AKTA purifier, cytiva, Buckinghamshire, England) equipped with polyetheretherketone (PEEK) tubing with an inner diameter of 0.25 mm. The mobile phase was degassed 1 mM TRIS buffer (pH 9.5). The injected sample pulse (500 µL of MNPs suspension with a particle concentration of 1 g/L) was pumped through the system while the effluent of the column was constantly analyzed by a flow-through UV absorbance measuring cell at λ 280 nm. In this way, MNP concentration could be monitored because we found a linear correlation between MNP concentration and absorbance (see Fig. S5). A fraction collector divided the effluent into samples for further analysis, each with a volume of 250 µL. The magnetic field source was switched on at the beginning of the experiment and a base flow rate of 2.6 *mL*/*min* was set, which corresponds to 38.00 *CV*/*h* considering the column's empty volume of 4.105 *mL*. After a volume of 6.00 *mL* (1.46 *CV*) had passed through the system, the magnetic field source was switched off and at the same time the flow rate was increased to 5.50 *mL*/*min* (80.39 *CV*/*h*). Single column experiments were performed at magnetic flux densities of 0.68 mT and 1.36 mT as well as without any external magnetic field influence. Peak areas, shapes as well as retention volumes were analyzed using the software Unicorn 5.2 (cytiva, Buckinghamshire, England).

3.2.2. SMB chromatography fractionation process

Experiments for continuous size fractionation of the investigated MNPs were executed with an AZURA Lab Simulated Moving Bed (SMB) system (Knauer Wissenschaftliche Gerate GmbH, Berlin, Germany). A SMB process approximates a continuous counter-current operation mode of a chromatographic system, in which the stationary phase moves in opposite direction to the mobile phase flow. The approximation is

technically realized by the use of four or more columns and a cyclic interchange of the feed and eluent inlet positions as well as raffinate and extract outlet positions by valve switching. If the flow rates of those in- and outflows along with the cycle time for valve switching are chosen carefully and correctly, a continuous MNP feed division into two effluent fractions can be achieved, resulting in a bimodal fractionation. As the process progresses, the species showing stronger interactions with the stationary phase will end up in the extract and the species showing weaker interactions will end up in the raffinate. Due to the increasing magnetic particle-matrix interactions with increasing particle diameter, the coarse material will be contained in the extract and the fine material in the raffinate, respectively. The whole system was equipped with PEEK tubing with an inner diameter of 0.7 mm. The flow rates are controlled by three piston pumps within the loop system and a feed pump which supplies the MNP suspension into the system, see Fig. 2. The flow directions are controlled by seven multi-position valves and by eight check valves. This arrangement would allow the integration of up to eight columns in the system, however, all SMB experiments were conducted by the use of four columns, one for each zone shown in Fig. 2. All columns were each equipped with an independently controllable magnetic coil. By controlling the four pumps, flow directions as well as flow rates within each zone could be adjusted independently. The flow rate differences required for successful fractionation in the four zones are additionally superimposed here by the application of external magnetic fields in zones 2 and 3. We chose this approach to optimize the process, as described above. For comparability reasons, SMB runs without magnetic field influence and with an magnetic flux density of 0.68 mT were performed. The process under magnetic field influence was executed twice in order to evaluate reproducibility and robustness. For each of the SMB runs, 1 mM TRIS (pH 9.5) served as eluent and 2 g/L nanomag-D MNP suspension, diluted in 1 mM TRIS, served as particle feed. The online analytics of extract and raffinate streams were performed using two UV measuring flow-through cells at λ 280 nm. Because of the periodical fluctuations of effluent concentrations, extract and raffinate samples were pooled over several complete switching cycles for further analyses by UV absorbance and DLS measurements in order to evaluate size fractionation quality.

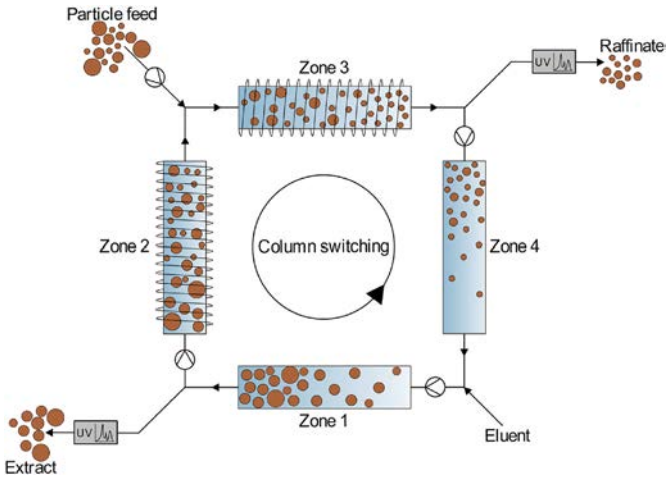

Fig. 2. Schematic illustration of the Simulated Moving Bed (SMB) chromatography process for fractionation of the particle feed into an extract and a raffinate fraction under magnetic field influence in SMB zones 2 and 3. The UV signal of both product streams is registered at λ = 280 nm. The flow rate varies in the four zones and external magnetic fields are applied onto the columns in zones 2 and 3. The column positions are switched periodically and counterclockwise.

3.3. SMB parameter selection

The flow rates in the individual SMB zones must be chosen carefully if the fractionation result shall be satisfactory. The findings obtained from single column experiments regarding flow rate dependencies were used for SMB process development. A common method to design a SMB process is the usage of the so-called Henry coefficients H_i of the substances to be separated and subsequent derivation of flow rate ratios [49]. The coefficients are derived from the retention volumes of the individual components:

$$H_i \quad \frac{\varepsilon}{1 \quad \varepsilon}\left(\frac{V_r}{\varepsilon\, V_{col} + V_{plant}} \quad 1\right) \tag{5}$$

with the column porosity ε, the respective component's retention volume V_r, the volume of the empty column V_{col} and the plant's dead volume V_{plant}. However, this classical approach of designing the SMB process was not applicable in the case of the size fractionation presented in this work. The polydisperse MNP suspension had a theoretically countless number of different species. Therefore, we defined a bimodal separation based on the two chromatogram peaks generated in single column experiments (see section 0). The respective first peak at the (lower) base flow rate $\dot{V}_{bf}$ thereby represented the weaker interacting component, i.e. the fine fraction. The second peak, which occurred after switching off the magnetic field source and/or increasing the flow rate to $\dot{V}_{hf}$ represented the more strongly interacting component, i.e. the coarse fraction. For this reason, only the Henry coefficient of the fine fraction H_{fine} corresponding to SMB zones 2 and 3 could be determined. Process conditions are modified when switching off the magnetic field source and therefore the flow rates for appropriate elution of the extract in zone 1 had to be determined experimentally. Furthermore, the SMB flow conditions can be captured using dimensionless flow rate ratios m_i [50]. These flow rate ratios m_i relate the flow rate of the mobile phase in the respective zone to the simulated flow rate of the stationary phase in the respective zone, with the latter resulting from switching the column positions counterclockwise:

$$m_i \quad \frac{\dot{V}_i\, t_s \quad V_{col}\, \varepsilon}{V_{col}\,(1 \quad \varepsilon)} \tag{6}$$

$\dot{V}_i$ denotes the flow rate of the mobile phase in the respective zone i, V_{col} is the volume of the column, t_s is the cyclic switching time of the system and ε is the porosity of the column packing.

The minimum base flow rate $\dot{V}_{bf,min}$ was determined in single column experiments and formulated as dimensionless flow rate ratio m_3 for SMB zone 3 (see Eq. (7)).

$$m_3 \quad \frac{\dot{V}_{bf}\, t_s \quad V_{col}\, \varepsilon}{V_{col}\,(1 \quad \varepsilon)} \tag{7}$$

The findings from the single column experiments thus provided important indications for the general feasibility as well as the key process parameters of the SMB setup. In order to ensure stable SMB process operation, the following conditions were compiled (derived in analogy to Refs. [50,51]):

$$\begin{aligned} & m_1 \geq m_3 \geq m_2 \geq H_{fine}\,; \\ & \quad m_4 \leq H_{fine}\,; \\ & m_3 \geq m_{3,min} \quad f\left(\dot{V}_{bf,min}\right) \end{aligned} \tag{8}$$

Given that the most important parameters (Henry coefficient of the fine fraction H_{fine}, minimum base flow rate $\dot{V}_{bf}$ and optimal magnetic flux density) could be determined via single column experiments, basic operation criteria for continuous multi-column chromatography could consequently be derived according to Eq. (7) and the boundary conditions in Eq. (8). The selected SMB process parameters are summarized in Table S2 in the SI.

3.4. Analytical methods

A dynamic light scattering (DLS) measurement device (Zetasizer Nano ZSP, Malvern Instruments, Malvern, England, detection range: 0.1 nm to 10 μm) was used to determine the PSDs of the MNP collectives in the respective fractions collected during single column and SMB experiments. PSD measurements were carried out in triplicate.

Absorbance of the fractions was recorded on a UV-VIS microplate reader (Tecan Spark, Tecan, Mannedorf, Switzerland) at a wavelength of λ 280 nm. A calibration curve was generated by applying linear regression to absorbance measurements at different MNP concentrations (R^2 0.9986, see Fig. S5). Subsequently, MNP concentration in each fraction was calculated using this calibration curve equation.

3.5. Evaluation of fractionation quality

A well-established method to assess the quality of a fractionation process is to generate a separation efficiency curve, also known as Tromp curve [52]. The value of the separation efficiency curve $T(\xi)$ at the point ξ is defined by the mass fraction of particles with a certain characteristic ξ, which end up in the coarse fraction. For this work, ξ represents the particle size. With this definition, $T(\xi)$ can be written as:

$$T(\xi) \quad \frac{z_{coarse}\, q_{coarse}(\xi)}{z_{feed}\, q_{feed}(\xi)} \quad \frac{z_{coarse}\, q_{coarse}(\xi)}{z_{coarse}\, q_{coarse}(\xi) + z_{fine}\, q_{fine}(\xi)} \tag{9}$$

with the respective mass fraction z_{coarse} as well as the density distribution q_{coarse} of the extract. z_{fine} denotes the mass fraction and q_{fine} the density distribution of the raffinate. The separation efficiency curve $T(\xi)$ can be used to derive a statement about the system's capability to separate two fractions satisfyingly. Having the separation efficiency curve $T(\xi)$, the separation sharpness κ can be defined as:

$$\kappa \quad \frac{\xi(T \quad 0.25)}{\xi(T \quad 0.75)} \tag{10}$$

with $\xi(T \quad 0.25)$ and $\xi(T \quad 0.75)$ being the particle property values at which the separation efficiency curve $T(\xi)$ reaches values of 0.25 and 0.75, respectively [53]. For instance, a separation sharpness κ higher than 0.6 is generally regarded as a sharp, technical separation in the field of particle technology [54].

4. Results and discussion

4.1. Single column studies

Preliminary to continuous SMB processing, single column fractionation experiments were carried out for parameter determination. In the runs shown here, a base flow rate of $\dot{V}_{bf}$ 2.60 mL/min was set, which corresponds to $\dot{V}_{bf}$ 38.0 CV/h and to a residence time in the column of τ 34.1 s. The increased flow rate $\dot{V}_{hf}$ had been adjusted to 5.5 mL/min (80.39 CV/h, τ 16.1 s). In order to examine the effect of the retention with an external magnetic field compared to a mechanism based just on the spontaneous single domain MNP magnetization, trials with two different magnetic flux densities and without any external magnetic field have been executed. The chromatograms resulting from those experiments are shown in Fig. 3. Retention volumes and peak areas are additionally summarized in the SI in Table S1.

In the execution without an externally applied magnetic field (dotted red curve), a sharp peak with a small shoulder at the front and modest tailing was observed at $\dot{V}_{bf}$. Emergence of this peak indicates that a significant amount of MNPs showed no retention on the matrix. Nevertheless, the second steep peak which occurred after increasing the flow rate to $\dot{V}_{hf}$ reveals that temporarily bound MNPs have been eluted. This effect is explained by the aforementioned spontaneous magnetization of the single domain MNPs. In the runs with an external field of

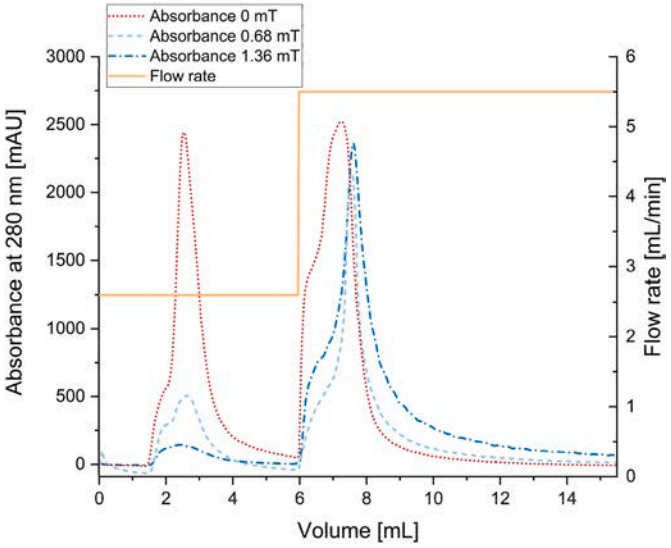

Fig. 3. Chromatograms of single column experiments. UV absorbance at λ = 280 nm (dotted red: no externally applied magnetic field; dashed, light blue: magnetic flux density of 0.68 mT was applied; dashed/dotted, intense blue: magnetic flux density of 1.36 mT was applied) was measured. The flow rate is depicted as the solid, orange line. Sample volumes of 500 μL each containing MNP suspension with a concentration of 1 g/L was injected. The respective magnetic field was switched off and simultaneously the flow rate was increased from 2.6 mL/min to 5.5 mL/min after a volume of 6 mL had elapsed. (For interpretation of the references to colour in this figure legend, the reader is referred to the Web version of this article.)

0.68 mT (dashed, light blue) and 1.36 mT (dashed/dotted, intense blue), significantly smaller peaks at $\dot{V}_{bf}$ were detected while the peak area decreased with increasing magnetic flux density. Since the magnetic effects of the fractionation matrix have been enhanced by applying an external field, more particles have been retained. Certainly, this effect even intensified with increasing magnetic flux density. Again, switching off the magnetic field source and increasing the flow rate to $\dot{V}_{hf}$ resulted in steep elution peaks. However, the respective peak maxima of the second peaks with external magnetic field were slightly delayed compared with the run without external magnetic influence (see also Table S1). This observation suggests that the retained particles may have adsorbed to the matrix already in the upper part of the column and were consequently eluted at a later point in time. Unexpectedly, coarse fraction peak areas were smaller compared to the run without magnetic field, which shows that probably not all loaded MNPs could be eluted at the selected flow rate $\dot{V}_{hf}$. For this reason, a higher flow rate than $\dot{V}_{hf}$ 5.5 mL/min had to be set in zone 1 in the SMB process in order to avoid permanent retention of MNPs on the column and to achieve the highest possible recovery. Assuming a homogenous particle density and ideally spherical MNPs, the respective volumetric median diameters (D_{50}) of the peak fractions collected during the single column experiments were determined via DLS measurements. The D_{50} values representing different sections during the three runs are shown in Fig. 4.

The median diameter generally increased throughout the fractionation experiments as expected, since bigger MNPs exhibited more intense interaction with the chromatography matrix than smaller ones [40]. A rapid and more or less steep increase in median diameter was observed in each run when we increased the flow rate to $\dot{V}_{hf}$. This fact is explained by the hydrodynamic drag force rising suddenly and exceeding the magnetic interactions of the MNPs with the chromatography matrix at this point as depicted in Fig. 1. In the case of fractionating the MNPs without applying an external magnetic field, only the magnetic interactions induced by spontaneous magnetization had to be overcome, therefore a much lower slope of the D_{50} curve and thus a less

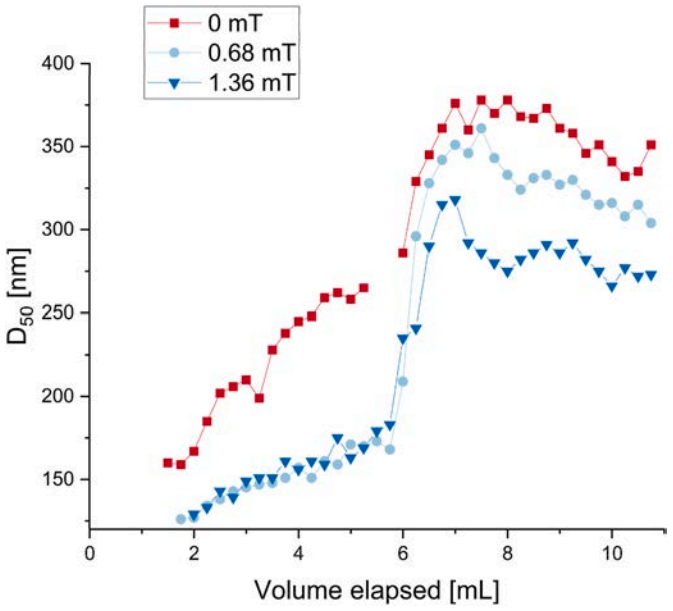

Fig. 4. DLS measurement results of the collected single column effluent samples of 250 µL each. The volumetric median diameters D_{50} are plotted against the volume which has passed the system. A sample volume of 500 µL containing a MNP suspension of 1 g/L was injected into the buffer feed stream. The external magnetic field source was switched off and the flow rate was increased from V_{bf} to V_{hf} simultaneously at V = 6 mL. Three different magnetic flux density conditions (0 mT, 0.68 mT, 1.36 mT) have been applied.

sharp separation curve was perceived (red square symbols in Fig. 4). Considering the increase in median diameter already in the first part ($\dot{V}_{bf}$) during the experiment, it is concluded that larger particles were decelerated by the matrix and consequently had higher retention volumes than small particles, which we had already shown in the previous study [40]. This effect already occurred without applying a magnetic field externally, which is again caused by the MNP's single domain nature. As soon as the flow rate was increased to $\dot{V}_{hf}$ at V 6 *mL*, even larger, strongly interacting, decelerated and even retained particles were eluted. For these runs under magnetic field influence, much steeper increases in D_{50} values were evident. During elution at $\dot{V}_{hf}$, clear differences between the lower (light blue circle symbols) and the higher (intense blue triangle symbols) magnetic flux densities could be recognized, with the higher magnetic flux density leading to smaller particle median diameters during elution. This difference is explained by the fact that the stronger magnetic interactions at 1.36 mT were able to retain smaller particles at $\dot{V}_{bf}$, which ultimately ended up in the coarse fraction. The most optimal size fractionation effect could therefore be found at a low magnetic flux density of 0.68 mT, which is why we selected this parameter value for the process transfer to the SMB system. Since the first peak showed a retention volume almost similar to the tracer peak retention volume, the Henry coefficient of the fine fraction was determined to H_{fine} 0.009, according to Eq. (5).

4.2. Simulated moving bed (SMB) chromatography experiments

The previously determined Henry coefficient of the fine fraction H_{fine}, minimum base flow rate $\dot{V}_{bf}$ and optimal magnetic flux density were used for the calculation of operation parameters for continuous multi-column chromatography, which can be found in the SI in Table S2. The MNP mass balance of feed, extract and raffinate streams revealed an overall recovery of 99.0% (w/w) in the execution without a magnetic field and of 99.9% (w/w) and 99.2% (w/w) in the executions with an external magnetic field.

Fig. 5A and B show the results of the MNP concentration analyses over the course of the SMB fractionation experiments. The yield values (black square symbols) fluctuated around 100% while exhibiting yield values <100% at the beginning of the processes in both cases. Thus, based on the absolute MNP concentration values (green and dashed pink columns) and the yield value in particular, it is apparent that the processes were characterized by a start-up behavior, although chromatography matrices were previously equilibrated. While this start-up phase took about 15–20 cycles when no magnetic field was applied, the process under magnetic field influence required only about eight to nine cycles to reach steady-state operation. The application of an external magnetic field thus allowed faster attainment of steady-state operation, which is caused by the larger differences between hydrodynamic and magnetic forces in the different SMB zones. Furthermore, when setting MNP concentrations in extract and raffinate side by side, almost balanced product mass fractions in the run with magnetic field (Fig. 5B and Table 1) were obtained. These results indicate that in the execution without magnetic field influence only a quite uneven distribution of the particle mass between the extract and raffinate streams was achieved. In the executions with an external field, the particle mass ratio of both product streams was approximately balanced. Furthermore, good inter-experimental reproducibility was proven in regards to extract and raffinate particle concentrations, as denoted in Table 1.

The PSDs were determined via DLS measurements and weighted to the respective mass fraction in order to derive the separation efficiency curves (see Eq. (9)) of the SMB runs with and without an external magnetic field. The weighted volume density distributions of the coarse and fine fraction as well as the separation efficiency curve (also called Tromp curve) are displayed for both SMB processes at steady-state operation in Fig. 6A and B.

Based on the generated separation efficiency curves it is stated that in both of the executions a fractionation by size of the MNP collective was achieved. Clear differences between the particle size distributions of coarse (extract) and fine (raffinate) fractions were obtained. To evaluate fractionation quality, the $D(T$ 0.25) and $D(T$ 0.75) values (see dashed grey lines) were used to calculate the separation sharpness κ. In the case of the execution without magnetic field (Fig. 6A), κ was 0.482, which still indicates a conventional, technical separation quality [53, 54]. However, this value was rather low compared to the experiment under external magnetic field influence (Fig. 6B) with a separation sharpness of 0.752. In addition, as already mentioned before, for the experiment without external magnetic field, there was an unbalanced particle concentration ratio between the fine and the coarse fraction (see Fig. 5A and Table 1). The weighting of the particle size distributions with the respective mass fractions therefore lead to distortions, and consequently, this separation efficiency curve only had limited validity here. On the other hand, the separation efficiency curve under magnetic field influence was very steep over its entire course and the MNP concentration ratio of the fine and coarse fraction was well balanced. Consequently, in this case the fractionation quality could be evaluated very reliably on the basis of the separation efficiency curve and the separation sharpness. The strong improvement of the separation quality compared to the execution without a magnetic field was primarily based on the more reliable retention of larger MNPs by applying an external magnetic field to SMB zones 2 and 3. As a result, the particle size distribution of the fine fraction exhibited significantly less tailing, which lead to a tightening of the separation efficiency curve, especially in the range of medium and large MNP sizes. Simultaneously, by using the external magnetic field, a very robust process had been developed, with a short start-up time of only a few cycles.

5. Conclusion

We investigated a novel method for continuous size fractionation of ultra-fine magnetic particles (MNPs). The competition of hydrodynamic and magnetic forces was identified as a significant influencing factor on

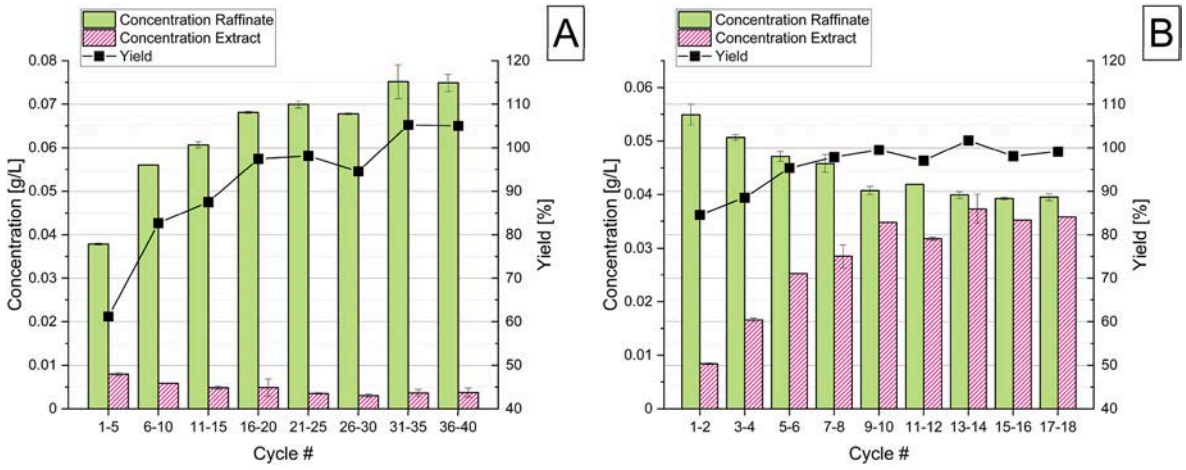

Fig. 5. Results of the particle concentration analyses of extract (pink hatched columns) and raffinate (green columns) product streams over the course of the SMB size fractionation experiments. The fractions were collected for five or two SMB cycles, respectively, and subsequently analyzed using UV absorbance measurements at $\lambda = 280$ nm in triplicate. The error bars indicate the standard deviations. The MNP mass balance revealed the yield values given as black symbols in both diagrams. A: execution without an external magnetic field; B: execution with a magnetic flux density of 0.68 mT. (For interpretation of the references to colour in this figure legend, the reader is referred to the Web version of this article.)

Table 1
Photometrically determined mass fractions z_{coarse} and z_{fine} of the extract and raffinate streams of the Simulated Moving Bed (SMB) experiments in %. (1) and (2) indicate the experiment number in the case of the repeated trial under magnetic field influence.

Magnetic flux density used in the respective experiment	z_{coarse} (extract) in %	z_{fine} (raffinate) in %
0.00 mT	5.2	94.8
0.68 mT (1)	48.7	51.3
0.68 mT (2)	46.5	53.5

the size-dependent particle retention in preliminary single-column studies. We successfully transferred the process to a Simulated Moving Bed chromatography system which led to very satisfying separation results even without an external magnetic field influence due to the MNP's magnetic single domain properties. Process robustness was significantly improved by local application of an external magnetic flux density of 0.68 mT. While providing a MNP recovery rate of 99.9% (w/w), separation sharpness was further increased to 0.752 in this case. These values indicate that nanoparticle fractionation using a modified SMB principle provides separations of a sharp, technical grade with the opportunity of uncomplicated scalability. A rapid attainment of steady-state operation combined with high efficiency demonstrated by a space-time yield of up to 2.94 g/(L*h) shows that this method constitutes a very promising approach for selective size fractionation of nanoscale magnetic particle systems on an industrial scale. By choosing correctly balanced process parameter sets, the resulting PSDs of the outlet streams could be easily adjusted, ranging from only the smallest particles ending up in the raffinate phase up to only the largest particles being fractionated into the extract phase, although it must be anticipated that for such extreme fractionations the yield can drop considerably. Accordingly, comparing with other alternative, commonly used fractionation methods, the investigated SMB system offers a continuous operation mode, easy scalability, a high space-time-yield and low energy consumption.

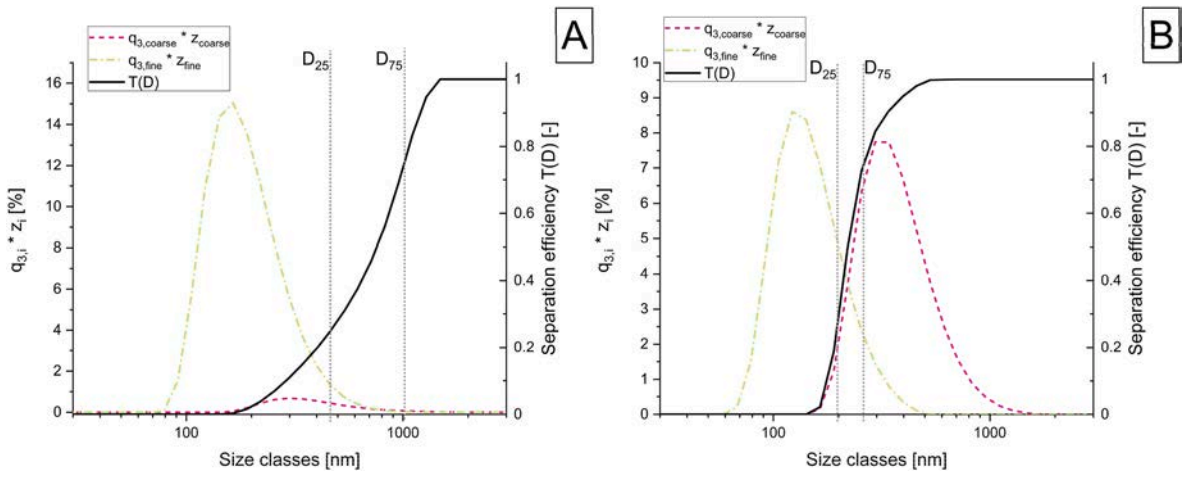

Fig. 6. Particle size distributions of the fine (raffinate, green dashed/dotted curves) and coarse (extract, pink dashed curves) fractions determined via DLS measurements. The volumetric size distributions $q_{3,i}$ were weighted by their respective particle mass fraction z_i (see Table 1). The separation efficiency curves T(D) were calculated using Eq. (9) and are given as solid black curves. The vertical, dashed grey lines signify the diameters at T = 0.25 and T = 0.75, which were used for separation sharpness calculation, see Eq. (10). A: execution without magnetic field; B: execution with an external magnetic flux density of 0.68 mT. (For interpretation of the references to colour in this figure legend, the reader is referred to the Web version of this article.)

Credit author statement

Laura Kuger: Investigation, Formal analysis, Writing – original draft; **Carsten-René Arlt**: Conceptualization, Investigation, Methodology, Writing – original draft; **Matthias Franzreb**: Writing – review & editing, Supervision, Funding acquisition.

Declaration of competing interest

The authors declare that they have no known competing financial interests or personal relationships that could have appeared to influence the work reported in this paper.

Acknowledgements

The authors gratefully acknowledge the financial support of the Deutsche Forschungsgemeinschaft (DFG). The work was done within the priority project SPP2045, subproject C11 (grant number FR 2131/6–2). Furthermore, the authors thank the company micromod Partikeltechnologie GmbH for kindly providing experimental material.

References

[1] T.A. Rocha-Santos, Sensors and biosensors based on magnetic nanoparticles, Trac. Trends Anal. Chem. 62 (2014) 28–36, https://doi.org/10.1016/j.trac.2014.06.016.
[2] K. Zhou, X. Zhou, J. Liu, Z. Huang, Application of magnetic nanoparticles in petroleum industry: a review, J. Petrol. Sci. Eng. 188 (2020) 106943, https://doi.org/10.1016/j.petrol.2020.106943.
[3] M. Franzreb, New classes of selective separations exploiting magnetic adsorbents, Curr. Opin. Colloid Interface Sci. 46 (2020) 65–76, https://doi.org/10.1016/j.cocis.2020.03.012.
[4] C. Scherer, A.M. Figueiredo Neto, Ferrofluids: properties and applications, Braz, J. Phys. 35 (2005) 718–727, https://doi.org/10.1590/S0103-97332005000400018.
[5] A.-H. Lu, W. Schmidt, N. Matoussevitch, H. Bonnemann, B. Spliethoff, B. Tesche, E. Bill, W. Kiefer, F. Schüth, Nanoengineering of a magnetically separable hydrogenation catalyst, Angew. Chem. 116 (2004) 4403–4406, https://doi.org/10.1002/ange.200454222.
[6] S.C. Tsang, V. Caps, I. Paraskevas, D. Chadwick, D. Thompsett, Magnetically separable, carbon-supported nanocatalysts for the manufacture of fine chemicals, Angew. Chem. 116 (2004) 5763–5767, https://doi.org/10.1002/ange.200460552.
[7] M. Govarthanan, C.-H. Jeon, Y.-H. Jeon, J.-H. Kwon, H. Bae, W. Kim, Non-toxic nano approach for wastewater treatment using Chlorella vulgaris exopolysaccharides immobilized in iron-magnetic nanoparticles, Int. J. Biol. Macromol. 162 (2020) 1241–1249, https://doi.org/10.1016/j.ijbiomac.2020.06.227.
[8] F. Gao, An overview of surface-functionalized magnetic nanoparticles: preparation and application for wastewater treatment, ChemistrySelect 4 (2019) 6805–6811, https://doi.org/10.1002/slct.201900701.
[9] Q.A. Pankhurst, J. Connolly, S.K. Jones, J. Dobson, Applications of magnetic nanoparticles in biomedicine, J. Phys. D Appl. Phys. 36 (2003) R167–R181, https://doi.org/10.1088/0022-3727/36/13/201.
[10] I. Raouf, J. Lee, H.S. Kim, M.-H. Kim, Parametric investigations of magnetic nanoparticles hyperthermia in ferrofluid using finite element analysis, Int. J. Therm. Sci. 159 (2021) 106604, https://doi.org/10.1016/j.ijthermalsci.2020.106604.
[11] C. Caizer, Optimization study on specific loss power in superparamagnetic hyperthermia with magnetite nanoparticles for high efficiency in alternative cancer therapy, Nanomaterials 11 (2020), https://doi.org/10.3390/nano11010040.
[12] J. Dobson, Magnetic nanoparticles for drug delivery, Drug Dev. Res. 67 (2006) 55–60, https://doi.org/10.1002/ddr.20067.
[13] R.P. Dhavale, R.P. Dhavale, S.C. Sahoo, P. Kollu, S.U. Jadhav, P.S. Patil, T. D. Dongale, A.D. Chougale, P.B. Patil, Chitosan coated magnetic nanoparticles as carriers of anticancer drug Telmisartan: pH-responsive controlled drug release and cytotoxicity studies, J. Phys. Chem. Solid. 148 (2021), 109749, https://doi.org/10.1016/j.jpcs.2020.109749.
[14] M. Grabowska, B.F. Grześkowiak, K. Rolle, R. Mrówczyński, Magnetic nanoparticles as a carrier of dsRNADouble-stranded RNA (dsRNA)for gene TherapyGene therapy, in: K. Narayanan (Ed.), BIO-CARRIER VECTORS: Methods and protocols, SPRINGER-VERLAG NEW YORK, [S.l., 2020, pp. 69–81.
[15] M. Hepel, Magnetic nanoparticles for nanomedicine, Magnetochemistry 6 (2020) 3, https://doi.org/10.3390/magnetochemistry6010003.
[16] A.-H. Lu, E.L. Salabas, F. Schüth, Magnetic nanoparticles: synthesis, protection, functionalization, and application, Angew. Chem. 46 (2007) 1222–1244, https://doi.org/10.1002/anie.200602866.
[17] T. Hyeon, Chemical Synthesis of Magnetic Nanoparticles, Chemical Communications, Cambridge, England, 2003, pp. 927–934, https://doi.org/10.1039/b207789b.
[18] H. Iida, K. Takayanagi, T. Nakanishi, T. Osaka, Synthesis of Fe3O4 nanoparticles with various sizes and magnetic properties by controlled hydrolysis, J. Colloid Interface Sci. 314 (2007) 274–280, https://doi.org/10.1016/j.jcis.2007.05.047.
[19] A.B. Chin, I.I. Yaacob, Synthesis and characterization of magnetic iron oxide nanoparticles via w/o microemulsion and Massart's procedure, J. Mater. Process. Technol. 191 (2007) 235–237, https://doi.org/10.1016/j.jmatprotec.2007.03.011.
[20] S. Sun, H. Zeng, Size-controlled synthesis of magnetite nanoparticles, J. Am. Chem. Soc. 124 (2002) 8204–8205, https://doi.org/10.1021/ja026501x.
[21] Y. Hou, H. Kondoh, T. Ohta, S. Gao, Size-controlled synthesis of nickel nanoparticles, Appl. Surf. Sci. 241 (2005) 218–222, https://doi.org/10.1016/j.apsusc.2004.09.045.
[22] Z. Surowiec, M. Budzyński, K. Durak, G. Czernel, Synthesis and characterization of iron oxide magnetic nanoparticles, Nukleonika 62 (2017) 73–77, https://doi.org/10.1515/nuka-2017-0009.
[23] S.P. Schwaminger, C. Syhr, S. Berensmeier, Controlled synthesis of magnetic iron oxide nanoparticles: magnetite or maghemite? Crystals 10 (2020) 214, https://doi.org/10.3390/cryst10030214.
[24] K. Chandra, V. Kumar, S.E. Werner, T.W. Odom, Separation of stabilized MOPS gold nanostars by density gradient centrifugation, ACS Omega 2 (2017) 4878–4884, https://doi.org/10.1021/acsomega.7b00871.
[25] M. Konrath, J. Gorenflo, N. Hübner, H. Nirschl, Application of magnetic bearing technology in high-speed centrifugation, Chem. Eng. Sci. 147 (2016) 65–73, https://doi.org/10.1016/j.ces.2016.03.025.
[26] F. Bonaccorso, M. Zerbetto, A.C. Ferrari, V. Amendola, Sorting nanoparticles by centrifugal fields in clean media, J. Phys. Chem. C 117 (2013) 13217–13229, https://doi.org/10.1021/jp400599g.
[27] M. Winkler, H. Sonner, M. Gleiss, H. Nirschl, Fractionation of ultrafine particles: evaluation of separation efficiency by UV–vis spectroscopy, Chem. Eng. Sci. 213 (2020) 115374, https://doi.org/10.1016/j.ces.2019.115374.
[28] S.-A. Lee, K.-H. Choo, C.-H. Lee, H.-I. Lee, T. Hyeon, W. Choi, H.-H. Kwon, Use of ultrafiltration membranes for the separation of TiO 2 photocatalysts in drinking water treatment, Ind. Eng. Chem. Res. 40 (2001) 1712–1719, https://doi.org/10.1021/ie000738p.
[29] A. Akthakul, A.I. Hochbaum, F. Stellacci, A.M. Mayes, Size fractionation of metal nanoparticles by membrane filtration, Adv. Mater. 17 (2005) 532–535, https://doi.org/10.1002/adma.200400636.
[30] M. Wu, Z. Mao, K. Chen, H. Bachman, Y. Chen, J. Rufo, L. Ren, P. Li, L. Wang, T. J. Huang, Acoustic separation of nanoparticles in continuous flow, Adv. Funct. Mater. 30 (2020) 2006375, https://doi.org/10.1002/adfm.202006375.
[31] K. Sandmann, U. Fritsching, Selektive partikelklassierung in ultraschallangeregten aerosolen, Chem. Ing. Tech. 92 (2020) 635–642, https://doi.org/10.1002/cite.201900158.
[32] M. Barasinski, G. Garnweitner, Restricted and unrestricted migration mechanisms of silica nanoparticles in agarose gels and their utilization for the separation of binary mixtures, J. Phys. Chem. C 124 (2020) 5157–5166, https://doi.org/10.1021/acs.jpcc.9b10644.
[33] P. Fraga García, M. Brammen, M. Wolf, S. Reinlein, M. Freiherr von Roman, S. Berensmeier, High-gradient magnetic separation for technical scale protein recovery using low cost magnetic nanoparticles, Separ. Purif. Technol. 150 (2015) 29–36, https://doi.org/10.1016/j.seppur.2015.06.024.
[34] S. Mirshahghassemi, A.D. Ebner, B. Cai, J.R. Lead, Application of high gradient magnetic separation for oil remediation using polymer-coated magnetic nanoparticles, Separ. Purif. Technol. 179 (2017) 328–334, https://doi.org/10.1016/j.seppur.2017.01.067.
[35] A.H. Latham, R.S. Freitas, P. Schiffer, M.E. Williams, Capillary magnetic field flow fractionation and analysis of magnetic nanoparticles, Anal. Chem. 77 (2005) 5055–5062, https://doi.org/10.1021/ac050611f.
[36] B. Kowalczyk, I. Lagzi, B.A. Grzybowski, Nanoseparations: strategies for size and/or shape-selective purification of nanoparticles, Curr. Opin. Colloid Interface Sci. 16 (2011) 135–148, https://doi.org/10.1016/j.cocis.2011.01.004.
[37] T. Ohara, S. Mori, Y. Oda, Y. Wada, O. Tsukamoto, Feasibility of magnetic chromatography for ultra-fine particle separation, IEEJ Trans.PE 116 (1996) 979–986, https://doi.org/10.1541/ieejpes1990.116.8_979.
[38] K.C. Karki, E.R. Whitby, S.V. Patankar, C. Winstead, T. Ohara, X. Wang, A numerical model for magnetic chromatography, Appl. Math. Model. 25 (2001) 355–373, https://doi.org/10.1016/S0307-904X(00)00057-3.
[39] M. Manouchehri, S. Seidi, F.O. Abdullah, Application of magnetic nanomaterials in magnetic-chromatography: a review, Talanta 229 (2021) 122273, https://doi.org/10.1016/j.talanta.2021.122273.
[40] C.-R. Arlt, A. Tschope, M. Franzreb, Size fractionation of magnetic nanoparticles by magnetic chromatography, J. Magn. Magn Mater. 497 (2020) 165967, https://doi.org/10.1016/j.jmmm.2019.165967.
[41] P. Satzer, M. Wellhoefer, A. Jungbauer, Continuous separation of protein loaded nanoparticles by simulated moving bed chromatography, J. Chromatogr. A 1349 (2014) 44–49, https://doi.org/10.1016/j.chroma.2014.04.093.
[42] C.-R. Arlt, D. Brekel, M. Franzreb, Continuous fractionation of nanoparticles based on their magnetic properties applying simulated moving bed chromatography,

Separ. Purif. Technol. 259 (2021) 118123, https://doi.org/10.1016/j.seppur.2020.118123.
[43] C.-R. Arlt, D. Brekel, S. Neumann, D. Rafaja, M. Franzreb, Continuous size fractionation of magnetic nanoparticles by using simulated moving bed chromatography, Front. Chem. Sci. Eng. https://doi.org/10.1007/s11705-021-2040-3.
[44] P. Biehl, M. von der Lühe, S. Dutz, F.H. Schacher, Synthesis, characterization, and applications of magnetic nanoparticles featuring polyzwitterionic coatings, Polymers 10 (2018), https://doi.org/10.3390/polym10010091.
[45] M. Ferreira, J. Sousa, A. Pais, C. Vitorino, The role of magnetic nanoparticles in cancer nanotheranostics, Materials 13 (2020), https://doi.org/10.3390/ma13020266.
[46] L.D. Tung, V. Kolesnichenko, D. Caruntu, N.H. Chou, C.J. O'Connor, L. Spinu, Magnetic properties of ultrafine cobalt ferrite particles, J. Appl. Phys. 93 (2003) 7486–7488, https://doi.org/10.1063/1.1540145.
[47] G.F. Goya, T.S. Berquó, F.C. Fonseca, M.P. Morales, Static and dynamic magnetic properties of spherical magnetite nanoparticles, J. Appl. Phys. 94 (2003) 3520–3528, https://doi.org/10.1063/1.1599959.
[48] R.M. Cornell, U. Schwertmann, The Iron Oxides: Structure, Properties, Reactions, Occurences and Uses, Wiley-VCH Verlag GmbH & Co. KGaA, Weinheim, 2003.
[49] C. Migliorini, M. Mazzotti, M. Morbidelli, Continuous chromatographic separation through simulated moving beds under linear and nonlinear conditions, J. Chromatogr. A 827 (1998) 161–173, https://doi.org/10.1016/S0021-9673(98)00643-8.
[50] A. Rajendran, G. Paredes, M. Mazzotti, Simulated moving bed chromatography for the separation of enantiomers, J. Chromatogr. A 1216 (2009) 709–738, https://doi.org/10.1016/j.chroma.2008.10.075.
[51] L.C. Kessler, A. Seidel-Morgenstern, Improving performance of simulated moving bed chromatography by fractionation and feed-back of outlet streams, J. Chromatogr. A 1207 (2008) 55–71, https://doi.org/10.1016/j.chroma.2008.08.022.
[52] A. Farzanegan, M. Gholami, M.H. Rahimian, Multiphase flow and tromp curve simulation of dense medium cyclones using Computational Fluid Dynamics, J. Mining Environ. 4 (2013) 67–76, https://doi.org/10.22044/jme.2013.142.
[53] S. Süß, C. Metzger, C. Damm, D. Segets, W. Peukert, Quantitative evaluation of nanoparticle classification by size-exclusion chromatography, Powder Technol. 339 (2018) 264–272, https://doi.org/10.1016/j.powtec.2018.08.008.
[54] H. Rumpf, Mechanische Verfahrenstechnik, Carl Hanser Verlag, München, Wien, 1975.